ELSEVIER

Journal of Power Sources 94 (2001) 92–96

JOURNAL OF POWER SOURCES

www.elsevier.com/locate/jpowsour

Study on the insertion behaviors of Lithium-ions into $CoFe_3Sb_{12}$ based electrodes

L.J. Zhang, X.B. Zhao*, X.B. Jiang, C.P. Lv, G.S. Cao

Department of Materials Science and Engineering, Zhejiang University, Hangzhou, 310027, PR China

Received 21 June 2000; received in revised form 20 September 2000; accepted 9 October 2000

Abstract

The electrochemical properties of multiphase $CoFe_3Sb_{12}$ based materials were studied with lithium anode model cell Li|LiPF$_6$ (EC + DMC) |$CoFe_3Sb_{12}$. A reversible capacity of about 490 mA h g^{-1} (ca. 3430 mA h cm^{-3}) has been obtained in the first cycle. The reversible capacity keeps above 240 mA h g^{-1} in the first 10 cycles. It was found that the cycle life and charge recovery are strongly dependent on particle size and conducting additive. The mechanism of lithium insertion into $CoFe_3Sb_{12}$ electrode was analyzed by ex situ XRD. It was found that there were two different types of the insertion reactions in the first discharge. One type is topotactic reaction and the other is reconstitution reaction. The chemical diffusion coefficient $\tilde{D}_{Li}$ versus lithium content x in $CoFe_3Sb_{12}$ has been examined by EIS for the first discharge.

Keywords: Anode materials; $CoFe_3Sb_{12}$; Electrochemical behavior; Lithium-ion batteries

1. Introduction

Lithium-ion batteries have had special attention in the recent years because they have a high energy density and are environmentally friendly. The conventional anode material of lithium-ion batteries, graphite, has a theoretical maximum capacity of 372 mA h g^{-1}, or a volumetric capacity of 800 A h l^{-1}, corresponding to the intercalation of one Li per six carbon atoms [1–5]. Tin oxides represent a new class of anode materials for Li-ion cells [6–10]. Idota et al. [11] have reported an amorphous tin-based composite oxide (TCO) which could be used instead of graphite and carbon as an anode material. Unfortunately, tin oxide-based anode materials have a large irreversible capacity resulting from the oxygen bonded to Sn that reacts with the Li to form Li_2O. This offsets the high reversible capacity advantage.

In recent years, there has been great interest in the study of alloys or intermetallic compounds with the aim of finding new materials for the negative electrode of lithium-ion cells such as Mg–Ge [12], Mg–Si [13], Sn–Fe [14], etc. They have much larger capacity for Li than graphite. For example, metallic Sb can electrochemically alloy with Li up to about three lithium atoms per one antimony atom.

We have studied the electrochemical properties of many kinds of thermoelectric materials such as Zn_4Sb_3 [15], Bi_2Te_3, $Bi_{0.5}Sb_{1.5}Te_3$. We found some of them could be the candidates for the anode materials for Lithium-ion batteries. $Co_{1-x}Fe_xSb_3$ ternary system is receiving detailed examination owing to its potential efficient thermoelectric behavior [16], and hence was studied in our series work to develop novel anode materials.

2. Experimental

$CoFe_3Sb_{12}$ was prepared as follows: stoichiometric amounts of the element powders (>98% pure) were sealed in a $\varnothing$ 14 mm × 100 mm quartz tube under vacuum (10^{-3} Pa). The tube was slowly heated up to 1100°C and holed at this temperature for 6 h, followed by quenching. Fine powders of $CoFe_3Sb_{12}$ were obtained by ball-milling the alloy for 120 h under the protection of ligroin with the mass ratio of the steel balls to powders being 20:1, and the rotation rate being 170 rpm followed by sieving with a 500-mesh screen. Coarse powders were obtained by artificial grinding followed by sieving with a 300-mesh screen.

X-ray diffraction (XRD) measurements were taken in a XD-98 diffractometer with Cu Kα_1 radiation by using step scans of 0.05° 2θ step from 20 to 70°. The ac impedance measurements were performed with a 1250 frequency

* Corresponding author. Fax: +86-571-7951152.
E-mail address: zhaoxb@cmsce.zju.edu.cn (X.B. Zhao).

0378-7753/01/$ – see front matter
PII: S0378-7753(00)00624-8

response analyzer combined with Solarton SI 1287 electrochemical interface. An alternating sinusoidal signal of 5 mV peak-to-peak was superimposed on the dc potential. The impedance spectra were obtained over a frequency range between 10^4 and 10^{-2} Hz.

All electrochemical measurements were carried out with lithium anode model cells. The cells were assembled in an Ar-filled glove box. Cathodes of $CoFe_3Sb_{12}$ were obtained by pressing the power, PTFE binder, and (or not) carbon black on a foam Ni substrate. The electrolyte was 1 M $LiPF_6$ in 50 vol.% EC (ethylene carbonate) and 50 vol.% DMC (dimethyl carbonate) solution. Cells were tested by cycling between 0.05 and 1.5 V at 30°C with a constant current of 20 mA g^{-1}.

3. Results and discussion

Fig. 1 gives the X-ray diffraction patterns of $CoFe_3Sb_{12}$ obtained by smelting at 1100°C. It can be seen that the alloy is multiphase structured with the dominated phases of Sb and $FeSb_2$. Some small components such as $CoSb_2$ can also be found in the XRD patterns.

The first discharge (insertion of Li^+) and charge (extraction of Li^+) curves of the $CoFe_3Sb_{12}$ samples are shown in Fig. 2 for sample A (coarse powers), sample B (fine powders), and sample C (fine powders with 10 wt.% carbon additives) (see Table 1 for details). The charge recovery and reversible capacity in the first cycle are 53% and 54 mA h g^{-1} for sample A, 44% and 260 mA h g^{-1} for sample B, 63% and 490 mA h g^{-1} for sample C, respectively. It can be noted the reversible capacity at the first cycle increases with the decrease of the particle size. It is well known that the insertion of lithium-ions into a metallic structure to form lithium-rich intermetallic phase such as Li_3Sb will increase the volume of the structure significantly and result in the pulverization of the electrode materials,

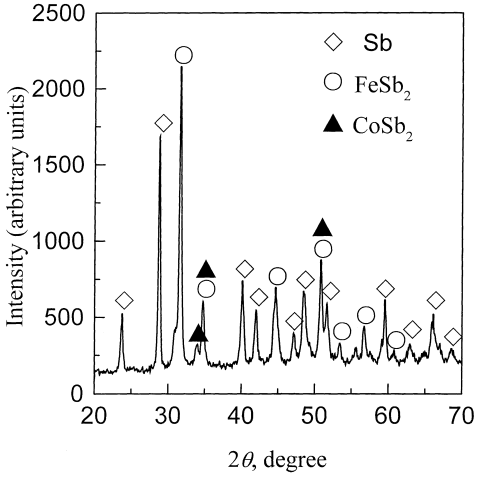

Fig. 1. $CoFe_3Sb_{12}$ XRD pattern using a XD-98 diffractometer with Cu $K\alpha_1$ radiation.

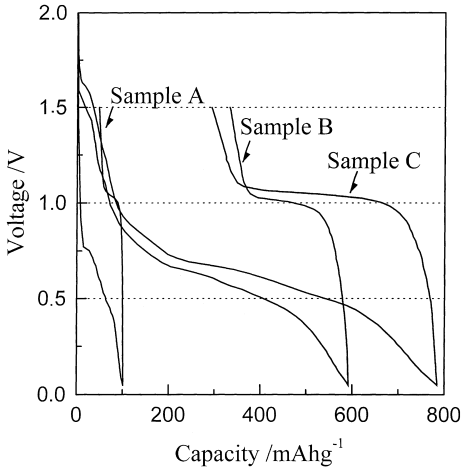

Fig. 2. Voltage profiles for the first circle for Li|$LiPF_6$ (EC + DMC) |$CoFe_3Sb_{12}$ cells: sample A: coarse powder; sample B: fine powder; sample C: fine powder with 10 wt.% carbon additives.

which would make some active materials be out of contact with the electrode and lead to the decrease of the charge recovery as well as the cycling capacity of the electrode. High disperse inert-conducting materials such as carbon black can increase the electrode conductivity and decrease the contact impedance in the electrode. Moreover, due to its good ductility, carbon black additives can hinder the divorcement of the active materials from the electrode caused by the violent volume change during the insertion and extraction of lithium-ions. One can find from Fig. 2 that both reversible capacity and charge recovery of sample C are much higher than that of samples A and B. In the following parts of the present work, the electrochemical behaviors of sample C will be discussed.

Fig. 3 gives the voltage profiles of the first five cycles for the Li|$LiPF_6$ (EC + DMC) |$CoFe_3Sb_{12}$ cell. It shows that the first discharge and charge capacity for the $CoFe_3Sb_{12}$ electrode are 785 and 490 mA h g^{-1}, respectively. The reversible capacity keeps above 240 mA h g^{-1} in the first 10 cycles. The cycling profiles indicate that the discharge capacity is larger than the charge capacities for each cycle. This implies that lithium is being trapped in the sample during cycling.

Fig. 4 shows the differential capacity versus voltage for the $CoFe_3Sb_{12}$ electrodes. A peak in the derivative curve corresponds to a plateau in the voltage profile in Fig. 3. From Fig. 4, one can see that the peak voltages of the second

Table 1
Composition of the electrodes used in the present work

Sample	Composition			
	Fine powder (wt.%)	Coarse powder (wt.%)	PTFE (wt.%)	Carbon black (wt.%)
A	–	97	3	–
B	97	–	3	–
C	82	–	8	10

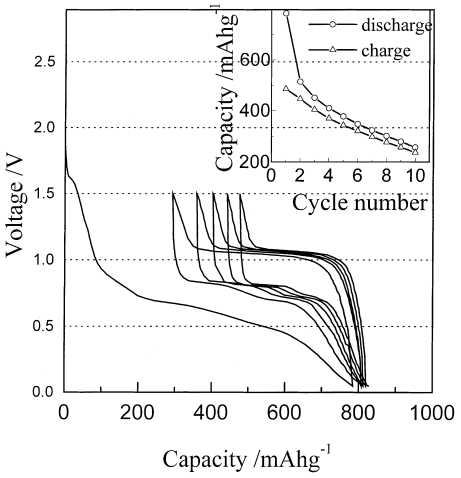

Fig. 3. Voltage profiles for the first five cycles of the cells with the $CoFe_3Sb_{12}$ anode (sample C).

discharge branches, 0.83 and 0.72 V, are significantly higher than those observed in the first discharge, 0.7 and 0.52 V. The differences suggest that there were different mechanisms of insertion of lithium-ions in the first cycle and the successive cycles. To investigate the mechanism for insertion/extraction of lithium-ions in $CoFe_3Sb_{12}$ anode material, the ex situ XRD analyses had been used.

Fig. 5 shows the ex situ XRD patterns of the $CoFe_3Sb_{12}$ electrode during the first cycle. The main Sb diffraction peaks cannot be observed in Fig. 5a (for pristine electrode, milled $CoFe_3Sb_{12}$ on foam Ni substrate) because the Sb particles become smaller by 120 h ball-milling, and the amount of alloy powder on Ni substrate is small during XRD analysis. In comparing with the pristine electrode (Fig. 5a), the diffraction peaks of $FeSb_2$ are slightly shifted to lower angles when the cell was discharged to 0.7 V (Fig. 5b). This means that the basic structural configurations of $FeSb_2$ remain essentially unchanged. After being

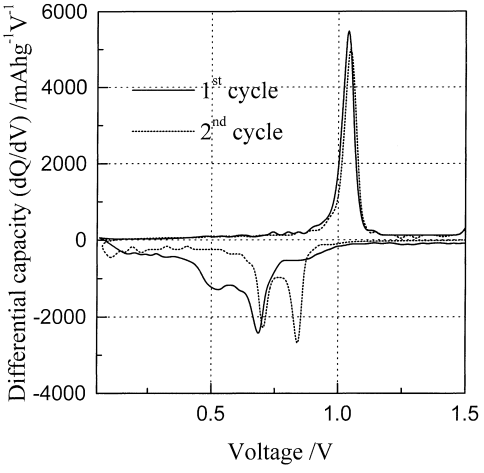

Fig. 4. Differential capacity vs. voltage for the $CoFe_3Sb_{12}$ (sample C) for the first and second cycles.

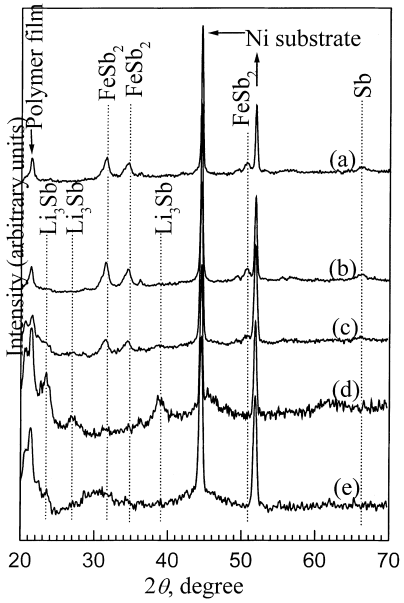

Fig. 5. Change in XRD patterns of $CoFe_3Sb_{12}$ (sample C) with different discharge–charge states at the first cycle: (a) fresh electrode; (b) discharged to 0.7 V; (c) discharged to 0.52 V; (d) discharged to 0.05 V; (e) charged to 1.5 V.

discharged to 0.52 V (Fig. 5c), the peak of Li_3Sb appears, while the peaks of $FeSb_2$ decreases. However, we are unable to identify the existence of Fe from XRD analyses. It suggests that the iron decomposed from $FeSb_2$ were too small or even amorphous, which are similar to the Fe–Sn sample reported by Mao et al. [14]. At the completely discharged state (Fig. 5d), $FeSb_2$ decomposes completely and the intensity of Li_3Sb peaks increases. The delithiation of the Li_3Sb alloy occurs during the charge, as the corresponding diffraction peaks decrease in intensity after the electrode was charged to 1.5 V. However, a small amount of Li_3Sb remains in the electrodes at 1.5 V. As a result, the charge capacity is significantly lower than the discharge capacity in the first cycle.

From the XRD analyses, we can suggest that there are two steps of processes during the first discharge. Lithium-ions insert into $FeSb_2$ lattices at first and form a kind of solid solution. This is a topotactic reaction, in which the mobile guest lithium-ions are inserted into or extracted from a static host crystal lattice $FeSb_2$, whose basic structural configuration remains essentially unchanged. With the increase of lithium insertion, the structural rearrangements with Li–Sb alloys being formed and $FeSb_2$ being consumed occur, which can be called reconstitution reaction according to Huggins [17]. At the successive charges and discharges, lithium-ions react with Sb reversibly.

An ac impedance analysis of $CoFe_3Sb_{12}$ during the first discharge is presented in Fig. 6. It could be found that the patterns include two parts: one is a no well-defined semicircle at high and intermediate frequencies, and the other is a straight line in the low frequency range corresponding to the Warburg impedance. The impedance values are adapted to a

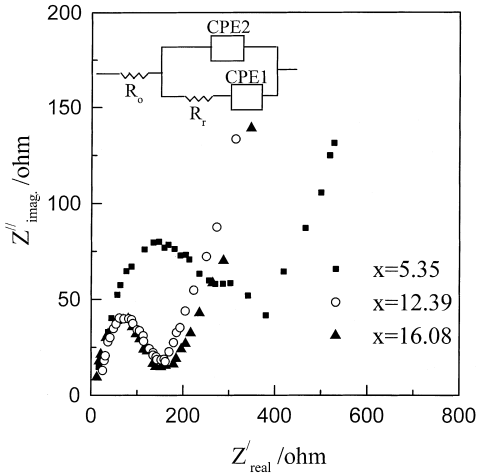

Fig. 6. An ac impedance of $CoFe_3Sb_{12}$ (sample C) at different x value (Li in $Li_xCoFe_3Sb_{12}$) during discharge at the first cycle: (a) $x = 5.35$; (b) $x = 12.39$; (c) $x = 16.08$.

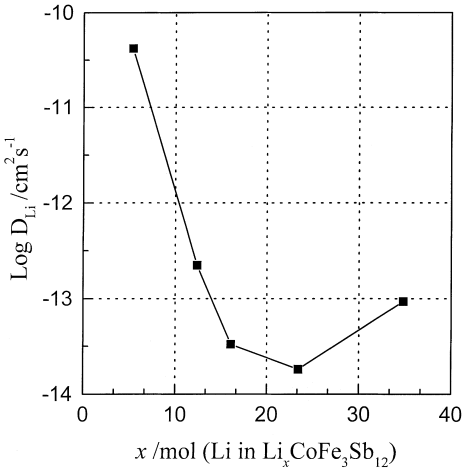

Fig. 8. Chemical diffusion coefficients $\tilde{D}_{Li}$ vary with x (insertion value of lithium-ions in the $CoFe_3Sb_{12}$ electrode at the first discharge).

proposed equivalent circuit model. $\tilde{D}_{Li}$, the chemical diffusion coefficient of lithium-ions in the $CoFe_3Sb_{12}$ electrode during the first discharge, was obtained by using the formula [18]

$$A = \frac{V_m}{\sqrt{2}nF}\frac{dE}{dx}\frac{1}{S\sqrt{\tilde{D}_{Li}}} \quad (1)$$

where A is Warburg coefficient, V_m the molar volume of the working electrode material, F the Faraday's constant, n the number of electrons transferred in the reaction, dE/dx the slope of the coulometric titration curve at each x value which can be calculated from coulometric titration curve in Fig. 7, and S the active surface.

Fig. 8 shows the calculated effects. We should notice that $\tilde{D}_{Li}$ derived from ac measurements here, represents only estimated value, because of the irreversible reactions in the first discharge and the inconsistent value of V_m during Li insertion. $\tilde{D}_{Li}$ varies between $10^{-11}$and 10^{-14} $cm^2\ s^{-1}$ for lithium-ion insertion content between $x \approx 5.35$ and 23.44 (x in $Li_xCoFe_3Sb_{12}$) which are corresponding to the voltage above 0.7 V (open potential versus Li^+/Li, which can be seen in Fig. 7). $\tilde{D}_{Li}$ gradually decreases until it reaches a minimum value for $x \approx 23.44$ in $Li_xCoFe_3Sb_{12}$, and increases again for $x \approx 34.8$ which corresponds to 0.69 V in Fig. 7. This means that the lithium diffusion rate decreases with the increase of the amount of lithium-ions in the composite electrode. The increase of $\tilde{D}_{Li}$ could be considered as the result of some structural modifications such as the formation of Li_2Sb nuclei.

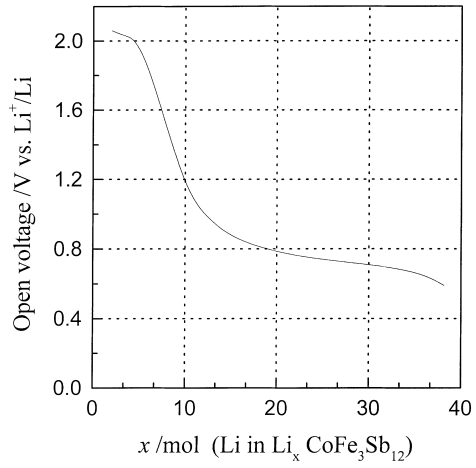

Fig. 7. Coulometric titration curve for Li|$LiPF_6$ (EC + DMC) |$CoFe_3Sb_{12}$ cell at the first discharge, which can be obtained by discharging the cell with 5 mA g^{-1} current and suspending at some certain x values (Li in $Li_xCoFe_3Sb_{12}$), take down the corresponding open voltages after 10 h.

4. Conclusion

The electrochemical properties of $CoFe_3Sb_{12}$ have been investigated using lithium anode model cells. The maximum discharge and charge capacity of 785 and 490 mA h g^{-1}, respectively, have been obtained in the first cycle. Decreasing particle size and addition of conducing additive can improve significantly the performance of $CoFe_3Sb_{12}$ electrode. Meanwhile, the insertion mechanism and kinetic parameters of $CoFe_3Sb_{12}$ have been analyzed with XRD and EIS. We propose that two different types of reactions occurred during the first discharges. One type is topotactic reaction and the other is reconstitution reaction. The chemical diffusion coefficient $\tilde{D}_{Li}$ decreased with x ($5.35 < x \leq 23.44$) in $Li_xCoFe_3Sb_{12}$ and increased at $x > 23.444$, corresponding to the structural modifications.

Acknowledgements

Project supported by National Natural Science Foundation of China (no. 59771032) and RFDP of the Education Ministry of China (no. 97033518).

References

[1] R. Fong, U.V. Sacken, J. Electrochem. Soc. 137 (7) (1990) 2009.
[2] N. Takami, A. Satoh, et al., J. Electrochem. Soc. 142 (2) (1995) 371.
[3] K. Tatumi, N. Iwashita, et al., J. Electrochem. Soc. 142 (3) (1995) 716.
[4] W. Xing, J.R. Dahn, J. Electrochem. Soc. 144 (4) (1997) 1195.
[5] K. Sato, M. Noguchi, et al., Science 264 (1994) 556.
[6] T. Brousse, R. Retoux, et al., J. Electrochem. Soc. 145 (1) (1998) 1.
[7] I.A. Courney, W.R. Mckinnon, J. Electrochem. Soc. 146 (1) (1999) 59.
[8] F. Ding, Z. Fu, et al., J. Electrochem. Soc. 146 (10) (1999) 3554.
[9] K. Wan, S.F.Y. Li, et al., J. Power Sources 75 (1998) 9.
[10] S.C. Nam, C.H. Paik, et al., J. Power Sources 84 (1999) 24.
[11] Y. Idota, T. Kabota, et al., Science 276 (30) (1997) 1395.
[12] H. Sakaguchi, H. Honda, et al., J. Power Sources 8182 (1999) 229.
[13] H. Kim, J. Choi, J. Electrochem. Soc. 146 (12) (1999) 4401.
[14] O. Mao, R.A. Dunlap, et al., J. Electrochem. Soc. 145 (12) (1998) 4195.
[15] X.B. Zhao, C.S. Cao, J. Mater. Sci. Lett. 19 (10) (2000) 851.
[16] J. Ackermann, A. Woldf, J. Phys. Chem. Solids 38 (1997) 1013.
[17] R.A. Huggins, J. Power Sources 276 (1997) 109.
[18] S. Colson, L.C. Klein, J. Electrochem. Soc. 139 (9) (1992) 2359.